Recent Advances on Mixed Metal Sulfides for Advanced Sodium-Ion Batteries

Yongjin Fang, Deyan Luan and Xiong Wen (David) Lou[*]

[*] Dr. Y. J. Fang, Dr. D. Y. Luan, Prof. X. W. Lou

School of Chemical and Biomedical Engineering, Nanyang Technological University, 62 Nanyang Drive, Singapore 637459, Singapore

Email: xwlou@ntu.edu.sg; davidlou88@gmail.com

Webpage: http://www.ntu.edu.sg/home/xwlou/

Abstract

Sodium-ion batteries (SIBs) have drawn enormous attention in the past few years from both academic and industrial battery communities in view of the fascinating advantages of rich abundance and low cost of sodium resources. Among various electrode materials, mixed metal sulfides (MMSs) stand out as promising negative electrode materials for SIBs considering their superior structural and compositional advantages, such as decent electrochemical reversibility, high electronic conductivity, and rich redox reactions. In this Progress Report, we summarize some recent developments in the rational design and synthesis of various kinds of MMSs with tailorable architectures, structural/compositional complexity, controllable morphologies, and enhanced electrochemical properties. The effect of structural engineering and compositional design of MMSs on the sodium storage properties is highlighted. It is anticipated that further innovative works on the material design of advanced electrodes for batteries can be inspired.

Keywords: mixed metal sulfides; heterostructures; chalcogenides; energy storage; sodium-ion batteries

1. Introduction

Sodium-ion batteries (SIBs) are being considered as one of the most appealing alternatives to lithium-ion batteries (LIBs) for grid-scale energy storage with intriguing features of infinite abundance and low cost of sodium resources and similar electrochemical reaction mechanisms to LIBs.[1-4] However, because of the larger ionic radius, higher reduction potential, and slower reaction kinetics of Na^+ ions compared to Li^+ ions, exploring electrodes with high reversible capacities and facile reaction processes remains challenging.[5-8] In the past few years, a wide range of promising materials has been developed as efficient electrode materials for SIBs, including cathode materials (e.g., polyanions,[9-12] transition metal oxides,[13-17] hexacyanoferrates[18, 19]) and anode materials (e.g., alloys,[20-26] metal chalcogenides,[27-32] carbonaceous materials[33-35]). It is noteworthy that the electrodes with two/multiple-electron reactions are more favored because of the high theoretical capacity for energy storage. Among these materials, metal sulfide anodes come into the spotlight due to the dazzling superiorities of high capacity and remarkable electrochemical reversibility.

By virtue of the advantageous features of diverse material species, compositions, crystalline phases, valence states, architectures, and controllable nanostructures/morphologies, metal sulfides manifest high electrochemical activity for sodium storage. Numerous metal sulfides have been applied for sodium storage and show promising electrochemical results.[36-38] Metal sulfides usually have higher electronic conductivity compared to metal oxide counterparts.[39, 40] And the bond energy of M-S in metal sulfides is weaker than the M-O in metal oxides, leading to faster kinetics during the conversion reactions.[41] Among the metal sulfides based electrode materials, mixed metal sulfides (MMSs) with mixture phases of different metal sulfides demonstrate richer redox reactions and higher electronic conductivity compared to the single-component metal sulfides, showing intrinsic advantages for sodium storage.[39] For MMSs, it is verified that the phase boundaries at the heterointerfaces can provide abundant lattice mismatches, distortions and defects, which have great influences on the charge carrier transport behavior by regulating the reaction kinetics and long-range

disorder.[42] Meanwhile, driven by the internal electric field at the heterointerfaces due to the dissimilar coupling components with different bandgaps, the interfacial reaction kinetics and electron/ion transport can be greatly promoted.[43] Additionally, owing to the synergetic effect of different components, the uniformly dispersed intermediate nanocrystals during electrochemical reactions can avoid the aggregation of generated metal nanoparticles thus obtaining good cyclability.[44] And the diverse redox potentials and out-of-step electrochemical reactions of different components would mitigate the strain during sodium uptake/extraction processes.[45] Therefore, it is inferred that MMSs with suitable compositions could achieve excellent electrochemical performance.

In general, the sodium storage mechanisms of metal sulfides are attributed to the combination of insertion, conversion, and/or alloying reactions.[37, 46, 47] During these reactions, the electrodes inevitably undergo severe volume change, which causes the collapse and pulverization of the structures and fading of capacity during repeated cycling. To address these issues, nanostructure engineering and compositing with conductive carbonaceous materials are reliable strategies for boosting the sodium storage properties of MMSs.[39] The nanostructured electrodes have several structure-dependent merits, resulting from the nanosized building units, large surface areas, and robust secondary configurations.[48-50] Specifically, the nanoscale permeable particles provide decreased diffusion energy barrier for electrons/Na^+ ions thus facilitate the reaction kinetics. The large surface area endows accessible electroactive sites and enables the full infiltration of electrolytes. And the elaborate architecture with tailored size and composition helps to retain the integrity of the electrode to achieve long-term cycle life.[51, 52] Moreover, the above promotive effects could be further facilitated through the integration of active materials with conductive carbonaceous materials.[53-55] The carbonaceous materials not only provide convenient electron/ion transportability for the hybrids but also exhibit excellent mechanical stability to effectively accommodate the severe volume variation during charge/discharge processes. Besides, it has been reported that metal doping in metal sulfides can introduce some lattice change (such as distortion, expansion and contraction), vacancies,

and electron deficiencies, which provide a facile path for sodium penetration into the host materials.[56] Therefore, nanostructure engineering and rational composition design on MMSs are believed to promote outstanding electrochemical properties from the considerations of improved electronic conductivity, accelerated ion transport, buffered volume change, and strengthened structural stability.

Although several review articles have provided comprehensive discussions on the application of metal sulfides for SIBs, they mainly focus on single-component metal sulfides.[37, 38, 41, 46, 57] Research efforts on the design and synthesis of MMSs for sodium storage have not been systemically surveyed. In this Progress Report, we summarize the recent advances of rationally designed MMSs with tailorable architectures, structural/compositional complexity, controllable morphologies, and enhanced sodium storage properties (**Figure 1**). First, we highlight the progress in the application of MMSs with simple compositions as anode materials in SIBs. Then, MMSs with complex compositions are thoroughly discussed, including integrating with carbonaceous materials and metal doping in MMSs. Finally, we will provide some brief conclusions and perspectives on the development of MMSs to inspire more innovative research on the design and fabrication of complex and rational MMSs for energy storage.

2. MMSs with simple compositions for SIBs

It has been demonstrated that mixed metal sulfides with synergistic effects of dissimilar components have shown better electrochemical properties compared to the single-component metal sulfides.[44, 58] More specifically, the heterostructures can lead to a promoted electron/ion transport pathway, and the diverse redox potentials and out-of-step electrochemical reactions of different components endow strengthened structural stability. For example, Veerasubramani et al. reported the fabrication of the $Fe_{1-x}S$/MnS nanocomposites through sulfidation of the Fe_2O_3/MnO_2 precursors.[58] The obtained $Fe_{1-x}S$/MnS nanocomposites show a longer lifespan and better rate capability compared to the individual $Fe_{1-x}S$ and MnS electrodes. These results may originate from the synergistic effects of different

components, controlled structural degradation, and enhanced pseudocapacitive contribution of the $Fe_{1-x}S$/MnS hybrids. Nanostructuring has been adopted to construct MMSs for boosted sodium storage performance.[42, 59, 60] Notably, yolk-shelled structures with distinctive hollow configurations can help to accelerate the reaction kinetics and buffer the volume variation of electrodes. Choi et al. reported the preparation of yolk-shelled SnS-MoS_2 microspheres through a spray pyrolysis process (**Figure 2**a, b).[44] The yolk-shelled SnS-MoS_2 microspheres exhibit much-improved cycling stability compared to the yolk-shelled SnS and MoS_2 and dense SnS-MoS_2. The yolk-shelled configuration offers a decreased Na^+ ion diffusion length and interspace for volume change, and uniformly dispersed SnS and MoS_2 nanocrystals avoid the metal aggregation during discharge thus to obtain good cyclability. Gu and co-workers demonstrated the fabrication of yolk-shelled Co_9S_8/MoS_2 spheres by a self-templating method (Figure 2c, d).[61] The as-formed yolk-shelled Co_9S_8/MoS_2 spheres exhibit superior sodium storage performance with a remarkable capacity of 300 mAh g^{-1} at 2 A g^{-1} after 1200 cycles. The in-depth investigation of phase boundaries on improved electrochemical properties was conducted by Liu and co-workers.[42] During the charge/discharge processes of yolk-shelled Bi_2S_3/MoS_2 heterostructure, the abundant phase boundaries generated from the recrystallization/redistribution of MoS_2 phase can alleviate the volume change and stabilize the Bi/Na_2S interface with uniform dispersion. As also confirmed by theoretical analysis, the abundant phase boundaries can induce a self-built-in electric field, resulting in boosted ion/electron transport pathway and improved reaction kinetics. As a result, the electrode exhibits high electrochemical reversibility with endurable Bi_2S_3/MoS_2 heterostructures. The Bi_2S_3/MoS_2 composites exhibit excellent cycling stability of 323 mAh g^{-1} after 1200 cycles at 10 A g^{-1}, which is much superior to the Bi_2S_3 and MoS_2 electrodes.

Besides the advantages of yolk-shelled structure, hierarchical hollow nanostructures with ultrathin 2D nanosheet subunits have shown remarkable superiority towards sodium storage.[62-65] In general, the thin permeable nanosheets can promote transport of the electrons/Na^+ ions and facilitate

the full infiltration of electrolyte, and the hollow structures guarantee the structural stability with effective accommodation of the stress during cycling.[66, 67] As a typical example, we recently have demonstrated the synthesis of hierarchical $CuS@CoS_2$ double-shelled nanoboxes (denoted as $CuS@CoS_2$ DSNBs) by using Cu_2O nanocubes as the precursor and template.[68] The multi-step synthesis procedure of the heterostructures is schematically shown in Figure 2e. Initially, a shell of $Co(OH)_2$ nanosheets is grown on Cu_2O nanocubes through the coordinating etching and precipitating reactions. Then, the obtained $Cu_2O@Co(OH)_2$ nanocubes are transferred to $Cu_2O@CuS@Co(OH)_2$ nanocubes through a selective sulfidation reaction. Afterward, the Cu_2O core in the $Cu_2O@CuS@Co(OH)_2$ nanocubes is selectively removed by an etching treatment to form the $CuS@Co(OH)_2$ nanoboxes. After the final solvothermal sulfidation reaction, the $CuS@Co(OH)_2$ nanoboxes are converted to $CuS@CoS_2$ DSNBs (Figure 2f-h). The CoS_2 nanosheets are strongly anchored on the CuS inner shell from the TEM observation (Figure 2i). With the unique structure of CoS_2 nanosheets on the CuS nanobox, the $CuS@CoS_2$ DSNBs exhibit good sodium storage performance in terms of high reversible capacity (625 mAh g^{-1} at 0.1 A g^{-1}), good rate capability (304 mAh g^{-1} at 5 A g^{-1}), and enhanced cycling stability (79% capacity retention after 500 cycles). The cyclability is much superior than the single-shelled CoS_2 and CuS nanoboxes and double-shelled $CuS@CoS_2$ nanoboxes with separated-layer structure (Figure 2j), indicating the vital effect of heterointerfaces on the electrochemical durability. A kinetics analysis based on the cyclic voltammogram test further indicates the characteristics of a capacitance-controlled behavior of the $CuS@CoS_2$ DSNBs.

3. MMSs with complex compositions for SIBs

To further enhance the structural stability and sodium storage performance of MMSs, numerous efforts have been devoted to tune the structures of MMSs. Efficient strategies, including compositing

with carbonaceous materials and metal doping in the structures, have been introduced to construct complex MMSs with boosted electrochemical properties.

3.1 MMSs with carbonaceous materials for SIBs

In general, integrating electrode materials with carbonaceous materials is an effective way to enhance sodium storage performance.[69] On the one hand, the superior electronic conductivity of carbonaceous materials endows the composites an efficient electron transport network to compensate for the insufficient electronic conductivity of metal sulfides. On the other hand, carbonaceous materials are ideal additives for relieving the large strain generated during repeated (de)sodiation processes and possibly suppress the shuttle effect of intermediate polysulfides in the electrolyte. Various carbonaceous materials with diversified structures, including pyrolytic carbon, carbon nanotubes, carbon cloth, and graphene, have been adopted to decorate the MMSs for efficient sodium storage.

The pyrolysis of polymers is a simple and efficient approach for preparing carbonaceous materials, which has been widely used to in situ decorate the MMSs. Various polymers, such as poly(styrene-acrylic) (PSA),[70] polydopamine (PDA),[71-75] poly(3, 4-ethylenedioxythiophene) (PEDOT),[76] polyacrylonitrile (PAN),[77] dextrin,[78] and polypyrrole (PPy)[79, 80] have been used as precursors to generate highly conductive carbon materials. For example, a carbon-coated Fe_9S_{10}@MoS_2 heterostructure was developed by Liu and co-workers.[81] The Fe_9S_{10} core with higher electronic conductivity could improve the electronic conductivity of the MoS_2 and facilitate the Na^+ ion transport due to the different reaction reversibility. Besides, the electric field at the heterointerface is strong because of the large bandgap difference of the Fe_9S_{10} (0 eV) and MoS_2 (1.17 eV), which can enhance electron/ion transport kinetics between the MoS_2 layer and the Fe_9S_{10} core (**Figure 3**a). X-ray absorption near-edge spectra of Fe L-edges and Mo M-edges confirm the increased interfacial structural disorder and improved charge-carrier mobility of the Fe_9S_{10}@MoS_2 heterostructure. DFT

calculations suggest that the energy barrier of Na^+ ions in the Fe_9S_{10}-MoS_2 heterostructure is much smaller than that in bare Fe_9S_{10} and MoS_2.With decreased ion diffusion energy barrier and reinforced geometry architecture, the heterointerfaces endow the hybrids fast charging/discharging capability and improved cycling stability. The Fe_9S_{10}@MoS_2@C electrode exhibits remarkable cyclability up to 1000 cycles with a high capacity retention of 93.4%. Kinetic analyses indicate that the Fe_9S_{10}@MoS_2@C exhibits a capacitive process with the largest Na^+ ion diffusion coefficient compared with the MoS_2@C and Fe_9S_{10}@C.

Furthermore, a rationally designed hierarchical nanocomposite with thin layer sandwiched carbon between the two metal sulfides may be an elaborate structure to obtain satisfying electrochemical performance. However, the synthesis of sandwiched carbon modified MMSs for sodium storage is rarely reported. Recently, we have designed and synthesized hierarchical three-layered Cu_2S@carbon@MoS_2 nanoboxes.[82] The overall synthetic route for the Cu_2S@carbon@MoS_2 hierarchical nanoboxes is schematically depicted in Figure 3b. Uniform Cu_2O nanocubes are used as self-templates to prepare CuS nanoboxes through the sequential sulfidation and etching processes. Next, Cu_2S@carbon nanoboxes are formed by coating a thin layer of PDA on the CuS nanoboxes followed by thermal annealing in N_2. Lastly, a layer of MoS_2 is grown on the Cu_2S@carbon nanoboxes through a solvothermal reaction to form the three-layered Cu_2S@carbon@MoS_2 hierarchical nanoboxes (Figure 3c-f). The rational design can efficiently promote the transport of electrons/Na^+ ions, buffer the volume variation of active materials, enhance the electronic conductivity of the composites, and maintain the structural stability for extended cycling. More specifically, compared to the normal carbon-integrated MMSs, the thin layer sandwiched carbon between two metal sulfides has some unique advantages. First, the sandwiched carbon can facilitate the electron transfer along the two metal sulfides, ensuring the high electronic conductivity of the hybrids. Second, the middle nitrogen-doped carbon could effectively separate the intermediates of different metal sulfides during electrochemical reactions, suppressing the

agglomeration of nanoparticles. Third, the flexible sandwiched carbon could well accommodate the volume change of the electrode materials, which helps to maintain the nanobox structures with enhanced structural stability. As a result, the Cu_2S@carbon@MoS_2 hierarchical microboxes demonstrate enhanced electrochemical properties in terms of high reversible capacity of 442 mAh g^{-1} and good rate capability of 297 mAh g^{-1} at 3 A g^{-1}.

Thanks to their tunable compositions and diverse structure, metal-organic frameworks (MOFs) have been widely utilized as precursors to prepare carbon-decorated MMSs.[45, 83-88] Specifically, the porous configuration and nanosized subunits of MOF-derived MMSs can provide high surface area and reduced diffusion length for Na^+ ions/electrons. And the pyrolysis of the heteroatom-containing ligand could generate heteroatom-doped carbon, guaranteeing high electronic conductivity of the hybrids. For example, Xiang et al. reported the formation of MoS_2/Co_9S_8/C nanoboxes by combining the solvothermal method and calcination process using the ZIF-67 template.[84] Due to the well-designed hybrid structures (Figure 3g and h), MoS_2/Co_9S_8/C composites manifest a high capacity of 546 mAh g^{-1} after 100 cycles at 0.5 A g^{-1} and a good rate capability of 222 mAh g^{-1} at 10 A g^{-1}. Using CoZn-MOFs as templates, nitrogen-doped carbon decorated Co_9S_8/ZnS nanocrystals were fabricated by Liang and co-workers.[45] A large amount of phase boundaries between ZnS and Co_9S_8 particles is observed from the HRTEM images. The abundant phase boundaries of Co_9S_8/ZnS provide numerous crystal defects and active sites for fast transport of electrons/Na^+ ions. The Co_9S_8/ZnS exhibits a larger capacitive contribution and a higher Na^+ diffusion coefficient compared to the monometal sulfides, suggesting the enhancement of ion diffusion and conductivity by the two mixed metal sulfides. The diverse redox potentials and out-of-step reactions of Co_9S_8 and ZnS nanocrystals would mitigate the strain during the charging/discharging processes, and the nitrogen-doped carbon with high conductivity can largely contribute to the pseudocapacitance effect. With these structural advantages, the Co_9S_8/ZnS exhibits a good rate capability of 258.6 mAh g^{-1} at 10 A g^{-1} and excellent stability up to 500 cycles. By coupling with polymer-derived pyrolytic carbon, the electrochemical

performance of MOF-derived MMSs can be greatly boosted. For example, ZnS-Sb_2S_3@C double-shelled polyhedrons synthesized via a sulfurization method combining a subsequent cation-exchange reaction are reported by Yin and co-workers (Figure 3i and j).[89] Owing to the high electronic conductivity and hollow configurations, the ZnS-Sb_2S_3@C polyhedrons can keep a high reversible capacity of 1029 mAh g^{-1} at 0.1A g^{-1} and retain a capacity of 630 mAh g^{-1} after 120 cycles.

Owing to the excellent conductivity, strong mechanical flexibility, and easy accessibility, different carbon matrixes including carbon cloth,[90, 91] carbon nanotubes,[92] and graphene,[93-97] have been adopted to decorate the MMSs. In this way, the conductivity of these MMSs could be greatly improved, the severe volume change could be efficiently accommodated, the structural integrity of active materials could be stabilized from the multicomponent synergy, and the ion/electron transfer is boosted via the built-in electric field. For example, Guan et. al fabricated coherent SnS_2/NiS_2 hetero-nanosheet arrays on carbon cloth (denoted as SnS_2/NiS_2@CC) (**Figure 4**a-d).[91] Because of the strong coupling effect of heterogeneous SnS_2/NiS_2 with a promoted transfer rate of electrons/Na^+ ions, reduced aggregation and volume variation, and 3D hierarchical nanostructures with accessible channels and highly conductive networks, the SnS_2/NiS_2@CC electrode demonstrates a high reversible capacity (857 mAh g^{-1} at 0.2 A g^{-1}) and good cycling stability (343.2 mAh g^{-1} at 2.0 A g^{-1} after 100 cycles). Besides, combining MMSs with graphene has been widely reported to promote the electrochemical performance of MMSs. SnS_2/Co_xS-rGO composites have been synthesized via the sulfidation of $CoSn(OH)_6$ precursors (Figure 4e-h).[98, 99] TEM investigations reveal that the $(SnCo)S_2$ heterostructures interlaced by highly elastic graphene nanosheets are highly stable. Besides, Co^0 nanoparticles formed at Sn^0/Na_2S heterointerface can serve as a barrier to avoid excessive diffusion of Sn^0 to the Sn^0/Na_2S interface thus resulting in better reversibility of continuous conversion/alloying reactions (Figure 4i).[99] As a result, the $(SnCo)S_2$/SG nanocubes manifest a high reversible capacity (758 mAh g^{-1} at 0.1 A g^{-1}) and excellent cycling stability (92.6% capacity retention at 5.0 A g^{-1} for 5000 cycles).

3.2 Metal-doped MMSs for SIBs

Metal doping is an effective approach for tuning the electrical properties of metal chalcogenide semiconductors and it has been widely used in the semiconductor industry.[100, 101] Doping a small amount of metal ions into the metal chalcogenides can lead to the minor lattice expansion/contraction of the structures, which results in higher mobility and more defect structures.[30, 56, 102] Thus, the metal doping can increase electronic conductivity and facilitate the Na^+ ion diffusion by decreasing the diffusion barrier. For example, Re-doped MoS_2 was reported to show improved electronic conductivity and more diffusion channels owing to the increased number of charge carriers and defect structures, leading to improved sodium storage properties.[103] However, the research on the synthesis of metal-doped MMSs for sodium storage is quite limited. Bera et al. reported the synthesis of dual-layered and doped heterostructures composed of SnS and Sn-doped Sb_2S_3 (denoted as SnS-Sn:Sb_2S_3) (**Figure 5**a and b).[104] With the improved kinetics, the SnS-Sn:Sb_2S_3 heterostructures maintain a high reversible capacity of 500 mAh g^{-1} after 50 cycles, which is much superior compared to the SnS and Sb_2S_3 samples (Figure 5c and d). Considering the distinctive merits of hollow architectures, the fabrication of metal-doped MMSs with hollow structures is expected to achieve decent sodium storage performance. We recently reported the fabrication of copper-doped CoS_2@Cu_xS double-shelled nanoboxes (denoted as Cu-CoS_2@Cu_xS DSNBs) via a sequential ion-exchange strategy (Figure 5e).[105] First, through a seeded epitaxial growth process, a layer of ZIF-8 is successfully grown on ZIF-67 nanocubes to obtain core-shelled ZIF-67@ZIF-8 polyhedrons. Then, the ZIF-67@ZIF-8 particles are transformed into CoS_2@ZnS DSNBs by a facile anion-exchange reaction. At last, the CoS_2@ZnS DSNBs are further converted to Cu-CoS_2@Cu_xS DSNBs by a cation-exchange process with copper ions. The Cu-CoS_2@Cu_xS DSNBs exhibit a well-defined polyhedral structure with hollow configurations (Figure 5f-i). Benefiting from the unique heterostructure and distinct hollow nanostructures, these Cu-CoS_2@Cu_xS DSNBs deliver a high capacity of 535 mAh g^{-1} at 0.1 A g^{-1}. Even at a high current density of 5 A g^{-1}, a high capacity of 333 mAh g^{-1} can be retained.

Besides, a long cycle life with 76% capacity retention over 300 cycles is achieved, which is much superior compared to the single-component metal sulfides (Figure 5j). The kinetic study based on CV offers further insight into the sodium storage behavior. The Cu-CoS_2@Cu_xS DSNBs exhibit capacitance-controlled characteristics, which is responsible for the superior rate performance. The high capacitive contribution may result from the heterostructures with nanoparticle-composed hollow configuration, which offers a large surface for the adsorption/desorption of Na^+ ions during repeated charge/discharge processes.

4. Summary and Outlook

In summary, this Progress Report provides an overview of the recent developments on the rational design and synthesis of mixed metal sulfides as high-performance electrode materials for sodium-ion batteries. It shows that great progress has been achieved in developing various types of mixed metal sulfides as anode materials for sodium storage, as summarized in **Table 1**. The advantageous effects of mixed metal sulfides and nanostructure engineering on their electrochemical properties are comprehensively discussed. The interfaces in mixed metal sulfides with a strong electric field enable fast charge carrier transport, leading to improved rate capability and cycling stability. Meanwhile, the rich phase boundaries could offer abundant defects and active sites for fast electron/ion transport. Besides, incorporation of carbonaceous materials with mixed metal sulfides can further enhance the electronic conductivity of the hybrids, provide an efficient buffering matrix/shell to mitigate large volume variation of electrode materials during the long-term cycling, and reduce the aggregation of active materials during synthesis and charge/discharge processes. Moreover, metal doping in metal sulfides could increase electronic conductivity and facilitate the Na^+ ion diffusion by decreasing the diffusion barrier. Of note, nanostructure engineering on mixed metal sulfides is an efficient way to boost the sodium storage performance, owing to decreased particle size to reduce the diffusion length of Na^+ ions/electrons, and exquisite architecture design in micro/nanoscale to improve the

geometrical stability and accommodate volume expansion. Additionally, a wide variety of metal sulfides can be incorporated into mixed metal sulfide combinations to satisfy a wide variety of design needs. Therefore, high reversible capacity, enhanced rate capability, and long-term cyclability can be achieved through the rationally designed mixed metal sulfide nanostructures.

Despite the encouraging progress, many challenges still exist for mixed metal sulfides to be optimized for practical sodium-ion batteries. While mixed metal sulfides show improved electrochemical properties compared to the single-component metal sulfides, how to choose different metal sulfides and integrate them into one united configuration remains challenging. The in-depth reaction mechanisms of mixed metal sulfides during (de)sodiation remain to be further investigated, especially how these heterostructures determine the charge transport and electrochemical kinetics are not yet fully understood. Some side reactions between electrolytes and intermediates and dissolution of polysulfides in electrolytes need to be suppressed. Developing feasible and cost-effective synthetic methods for high-performance mixed metal sulfide electrodes remains a big challenge. In addition, more complex structures, such as ternary/quaternary metal sulfides might be further studied. Furthermore, the intrinsic relationships between nanostructured mixed metal sulfide materials and their electrochemical properties await extensive investigation via advanced *in-situ*/*ex-situ* characterization and theoretical calculations. Although many mixed metal sulfides show excellent sodium storage performance in half cells, it is expected to see more studies about their application in full cells/prototype batteries. For prototype batteries, the higher voltage behavior of MMSs based anodes would make a safer battery than one with alloy or carbonaceous anodes, but at the same time it becomes necessary to find high-voltage cathode materials that can match with MMSs to achieve full batteries with high output energy density. Besides, the adoption of earth-abundant and non-toxic raw materials (e.g., Mn-based and Fe-based MMSs) and green manufacturing processes are more favored considering the cost-effectiveness and environmental issues.

With continuous studies on the mixed metal sulfides for sodium-ion batteries and growing interest from battery communities, we anticipate that mixed metal sulfides will play a vital role in energy storage applications in view of the unique structural and compositional features. It is optimistic that more advanced mixed metal sulfide electrode materials will be designed towards grid-scale energy storage applications with high energy/power density in the future.

Acknowledgments

X. W. L. acknowledges the funding support from the National Research Foundation (NRF) of Singapore via the NRF investigatorship (NRF-NRFI2016-04) and Ministry of Education of Singapore via the Academic Research Fund (AcRF) Tier-1 Funding (RG116/18).

References

[1] C. Vaalma, D. Buchholz, M. Weil, S. Passerini, *Nat. Rev. Mater.* **2018**, *3*, 18013.

[2] J.-Y. Hwang, S.-T. Myung, Y.-K. Sun, *Chem. Soc. Rev.* **2017**, *46*, 3529.

[3] Y. Fang, X.-Y. Yu, X. W. Lou, *Matter* **2019**, *1*, 90.

[4] Y. Sun, S. Guo, H. Zhou, *Adv. Energy Mater.* **2019**, *9*, 1800212.

[5] L. Li, Y. Zheng, S. Zhang, J. Yang, Z. Shao, Z. Guo, *Energy Environ. Sci.* **2018**, *11*, 2310.

[6] S. Chou, Y. Yu, *Adv. Energy Mater.* **2017**, *7*, 1703223.

[7] H. Kim, H. Kim, Z. Ding, M. H. Lee, K. Lim, G. Yoon, K. Kang, *Adv. Energy Mater.* **2016**, *6*, 1600943.

[8] E. Lim, C. Jo, M. S. Kim, M.-H. Kim, J. Chun, H. Kim, J. Park, K. C. Roh, K. Kang, S. Yoon, J. Lee, *Adv. Funct. Mater.* **2016**, *26*, 3711.

[9] Y. Fang, J. Zhang, L. Xiao, X. Ai, Y. Cao, H. Yang, *Adv. Sci.* **2017**, *4*, 1600392.

[10] X. Rui, W. Sun, C. Wu, Y. Yu, Q. Yan, *Adv. Mater.* **2015**, *27*, 6670.

[11] Y. Fang, L. Xiao, X. Ai, Y. Cao, H. Yang, *Adv. Mater.* **2015**, *27*, 5895.

[12] Y. Fang, Q. Liu, L. Xiao, Y. Rong, Y. Liu, Z. Chen, X. Ai, Y. Cao, H. Yang, J. Xie, C. Sun, X. Zhang, B. Aoun, X. Xing, X. Xiao, Y. Ren, *Chem* **2018**, *4*, 1167.

[13] P.-F. Wang, H.-R. Yao, X.-Y. Liu, Y.-X. Yin, J.-N. Zhang, Y. Wen, X. Yu, L. Gu, Y.-G. Guo, *Sci. Adv.* **2018**, *4*, eaar6018.

[14] Y. Wang, X. Yu, S. Xu, J. Bai, R. Xiao, Y.-S. Hu, H. Li, X.-Q. Yang, L. Chen, X. Huang, *Nat. Commun.* **2013**, *4*, 1.

[15] Y. Cao, L. Xiao, W. Wang, D. Choi, Z. Nie, J. Yu, L. V. Saraf, Z. Yang, J. Liu, *Adv. Mater.* **2011**, *23*, 3155.

[16] Y.-F. Zhu, Y. Xiao, W.-B. Hua, S. Indris, S.-X. Dou, Y.-G. Guo, S.-L. Chou, *Angew. Chem. Int. Ed.* **2020**, *59*, DOI: 10.1002/anie.201915650.

[17] Y. Fang, X.-Y. Yu, X. W. Lou, *Angew. Chem. Int. Ed.* **2017**, *56*, 5801.

[18] J. Qian, C. Wu, Y. Cao, Z. Ma, Y. Huang, X. Ai, H. Yang, *Adv. Energy Mater.* **2018**, *8*, 1702619.

[19] K. Hurlbutt, S. Wheeler, I. Capone, M. Pasta, *Joule* **2018**, *2*, 1950.

[20] M. Lao, Y. Zhang, W. Luo, Q. Yan, W. Sun, S. X. Dou, *Adv. Mater.* **2017**, *29*, 1700622.

[21] H. Zhang, I. Hasa, S. Passerini, *Adv. Energy Mater.* **2018**, *8*, 1702582.

[22] Y. Fang, X.-Y. Yu, X. W. Lou, *Angew. Chem. Int. Ed.* **2018**, *57*, 9859.

[23] S. Yuan, Y.-H. Zhu, W. Li, S. Wang, D. Xu, L. Li, Y. Zhang, X.-B. Zhang, *Adv. Mater.* **2017**, *29*, 1602469.

[24] X. Fan, J. Mao, Y. Zhu, C. Luo, L. Suo, T. Gao, F. Han, S.-C. Liou, C. Wang, *Adv. Energy Mater.* **2015**, *5*, 1500174.

[25] Z. Li, X. Tan, P. Li, P. Kalisvaart, M. T. Janish, W. M. Mook, E. J. Luber, K. L. Jungjohann, C. B. Carter, D. Mitlin, *Nano Lett.* **2015**, *15*, 6339.

[26] D. Kim, K. Zhang, M. Cho, Y.-M. Kang, *Energy Environ. Sci.* **2019**, *12*, 1326.

[27] Z. Li, J. Zhang, Y. Lu, X. W. Lou, *Sci. Adv.* **2018**, *4*, eaat1687.

[28] X. Wei, X. Wang, X. Tan, Q. An, L. Mai, *Adv. Funct. Mater.* **2018**, *28*, 1804458.

[29] C. Wu, Y. Jiang, P. Kopold, P. A. van Aken, J. Maier, Y. Yu, *Adv. Mater.* **2016**, *28*, 7276.

[30] Y. Fang, X.-Y. Yu, X. W. Lou, *Adv. Mater.* **2018**, *30*, 1706668.

[31] Z. Li, K. Jiang, F. Khan, A. Goswami, J. Liu, A. Passian, T. Thundat, *Sci. Adv.* **2019**, *5*, eaav2820.

[32] K. Zhang, Z. Hu, X. Liu, Z. Tao, J. Chen, *Adv. Mater.* **2015**, *27*, 3305.

[33] Y. Cao, L. Xiao, M. L. Sushko, W. Wang, B. Schwenzer, J. Xiao, Z. Nie, L. V. Saraf, Z. Yang, J. Liu, *Nano Lett.* **2012**, *12*, 3783.

[34] Z. Li, C. Bommier, Z. S. Chong, Z. Jian, T. W. Surta, X. Wang, Z. Xing, J. C. Neuefeind, W. F. Stickle, M. Dolgos, *Adv. Energy Mater.* **2017**, *7*, 1602894.

[35] H. Hou, X. Qiu, W. Wei, Y. Zhang, X. Ji, *Adv. Energy Mater.* **2017**, *7*, 1602898.

[36] Y. Liu, X.-Y. Yu, Y. Fang, X. Zhu, J. Bao, X. Zhou, X. W. Lou, *Joule* **2018**, *2*, 725.

[37] Y. Xiao, S. H. Lee, Y. K. Sun, *Adv. Energy Mater.* **2017**, *7*, 1601329.

[38] Z. Ali, T. Zhang, M. Asif, L. Zhao, Y. Yu, Y. Hou, *Mater. Today* **2020**, DOI: 10.1016/j.mattod.2019.11.008.

[39] X. Y. Yu, X. W. Lou, *Adv. Energy Mater.* **2018**, *8*, 1701592.

[40] X.-Y. Yu, L. Yu, X. W. Lou, *Adv. Energy Mater.* **2016**, *6*, 1501333.

[41] S. Dai, L. Wang, M. Cao, Z. Zhong, Y. Shen, M. Wang, *Mater. Today Energy* **2019**, *12*, 114.

[42] L. Cao, X. Liang, X. Ou, X. Yang, Y. Li, C. Yang, Z. Lin, M. Liu, *Adv. Funct. Mater.* **2020**, *30*, 1910732.

[43] C. Zhang, F. Han, J. Ma, Z. Li, F. Zhang, S. Xu, H. Liu, X. Li, J. Liu, A.-H. Lu, *J. Mater. Chem. A* **2019**, *7*, 11771.

[44] S. H. Choi, Y. C. Kang, *ACS Appl. Mater. Interfaces* **2015**, *7*, 24694.

[45] G. Fang, Z. Wu, J. Zhou, C. Zhu, X. Cao, T. Lin, Y. Chen, C. Wang, A. Pan, S. Liang, *Adv. Energy Mater.* **2018**, *8*, 1703155.

[46] Y. Liu, C. Yang, Q. Zhang, M. Liu, *Energy Storage Mater.* **2019**, *22*, 66.

[47] E. Cho, K. Song, M. H. Park, K.-W. Nam, Y.-M. Kang, *Small* **2016**, *12*, 2510.

[48] P. He, Y. Fang, X.-Y. Yu, X. W. Lou, *Angew. Chem. Int. Ed.* **2017**, *56*, 12202.

[49] S. Wang, Y. Fang, X. Wang, X. W. Lou, *Angew. Chem. Int. Ed.* **2019**, *58*, 760.

[50] F. Li, Z. Zhou, *Small* **2018**, *14*, 1702961.

[51] F. Xie, L. Zhang, C. Ye, M. Jaroniec, S.-Z. Qiao, *Adv. Mater.* **2019**, *31*, 1800492.

[52] Y. Fang, X.-Y. Yu, X. W. Lou, *Angew. Chem. Int. Ed.* **2019**, *58*, 7744.

[53] Y. Liu, Y. Fang, Z. Zhao, C. Yuan, X. W. Lou, *Adv. Energy Mater.* **2019**, *9*, 1803052.

[54] Z. Li, Y. Fang, J. Zhang, X. W. Lou, *Adv. Mater.* **2018**, *30*, 1800525.

[55] C. Dong, L. Guo, H. Li, B. Zhang, X. Gao, F. Tian, Y. Qian, D. Wang, L. Xu, *Energy Storage Mater.* **2020**, *25*, 679.

[56] K. Zhang, M. Park, L. Zhou, G.-H. Lee, J. Shin, Z. Hu, S.-L. Chou, J. Chen, Y.-M. Kang, *Angew. Chem. Int. Ed.* **2016**, *55*, 12822.

[57] Z. Hu, Q. Liu, S. L. Chou, S. X. Dou, *Adv. Mater.* **2017**, *29*, 1700606.

[58] G. K. Veerasubramani, M.-S. Park, J.-Y. Choi, Y.-S. Lee, S. J. Kim, D.-W. Kim, *ACS Sustainable Chem. Eng.* **2019**, *7*, 5921.

[59] J. Zhong, X. Xiao, Y. Zhang, N. Zhang, M. Chen, X. Fan, L. Chen, *J. Alloys Compd.* **2019**, *793*, 620.

[60] H. Zhou, Y. Zhang, Y. Cao, X. Zhou, *Mater. Lett.* **2019**, *238*, 222.

[61] H. Geng, J. Yang, Z. Dai, Y. Zhang, Y. Zheng, H. Yu, H. Wang, Z. Luo, Y. Guo, Y. Zhang, *Small* **2017**, *13*, 1603490.

[62] D. Xu, W. Chen, M. Zheng, X. Huang, Y. Fang, X. Yu, *Electrochim. Acta* **2018**, *265*, 419.

[63] Y. Zhang, C. W. Foster, C. E. Banks, L. Shao, H. Hou, G. Zou, J. Chen, Z. Huang, X. Ji, *Adv. Mater.* **2016**, *28*, 9391.

[64] Y. Xiao, D. Su, X. Wang, S. Wu, L. Zhou, Y. Shi, S. Fang, H.-M. Cheng, F. Li, *Adv. Energy Mater.* **2018**, *8*, 1800930.

[65] J. Zhou, L. Wang, M. Yang, J. Wu, F. Chen, W. Huang, N. Han, H. Ye, F. Zhao, Y. Li, *Adv. Mater.* **2017**, *29*, 1702061.

[66] Y. Lu, L. Yu, X. W. Lou, *Chem* **2018**, *4*, 972.

[67] W. Zhao, C. Guo, C. M. Li, *J. Mater. Chem. A* **2017**, *5*, 19195.

[68] Y. Fang, B. Y. Guan, D. Luan, X. W. Lou, *Angew. Chem. Int. Ed.* **2019**, *58*, 7739.

[69] P. Geng, S. Zheng, H. Tang, R. Zhu, L. Zhang, S. Cao, H. Xue, H. Pang, *Adv. Energy Mater.* **2018**, *8*, 1703259.

[70] H. Xie, M. Chen, L. Wu, *ACS Appl. Mater. Interfaces* **2019**, *11*, 41222.

[71] Y. Lin, Z. Qiu, D. Li, S. Ullah, Y. Hai, H. Xin, W. Liao, B. Yang, H. Fan, J. Xu, C. Zhu, *Energy Storage Mater.* **2018**, *11*, 67.

[72] Y. Zhang, P. Wang, Y. Yin, N. Liu, N. Song, L. Fan, N. Zhang, K. Sun, *Carbon* **2019**, *150*, 378.

[73] J. Chen, S. Li, V. Kumar, P. S. Lee, *Adv. Energy Mater.* **2017**, *7*, 1700180.

[74] J. H. Choi, S.-K. Park, Y. C. Kang, *Chem. Eng. J.* **2020**, *383*, 123112.

[75] X. Ou, L. Cao, X. Liang, F. Zheng, H.-S. Zheng, X. Yang, J.-H. Wang, C. Yang, M. Liu, *ACS Nano* **2019**, *13*, 3666.

[76] J. Ai, X. Zhao, Y. Lei, S. Yang, Q. Xu, C. Lai, C. Peng, *Appl. Surf. Sci.* **2019**, *496*, 143631.

[77] C. Chen, G. Li, J. Zhu, Y. Lu, M. Jiang, Y. Hu, Z. Shen, X. Zhang, *Carbon* **2017**, *120*, 380.

[78] J.-S. Park, Y. Chan Kang, *J. Mater. Chem. A* **2017**, *5*, 8616.

[79] L. Cao, B. Zhang, X. Ou, C. Wang, C. Peng, J. Zhang, *Small* **2019**, *15*, 1804861.

[80] Y. Wang, W. Kang, P. Ma, D. Cao, D. Cao, Z. Kang, D. Sun, *Mater. Chem. Front.* **2020**, *4*, 1212.

[81] C. Zhang, F. Han, F. Wang, Q. Liu, D. Zhou, F. Zhang, S. Xu, C. Fan, X. Li, J. Liu, *Energy Storage Mater.* **2020**, *24*, 208.

[82] Y. Fang, D. Luan, Y. Chen, S. Gao, X. W. Lou, *Angew. Chem. Int. Ed.* **2020**, *59*, 7178.

[83] D. Cao, W. Fan, W. Kang, Y. Wang, K. Sun, J. Zhao, Z. Xiao, D. Sun, *Mater. Today Energy* **2019**, *12*, 53.

[84] J. Xiang, T. Song, *Chem. Commun.* **2017**, *53*, 10820.

[85] X. Liu, F. Zou, K. Liu, Z. Qiang, C. J. Taubert, P. Ustriyana, B. D. Vogt, Y. Zhu, *J. Mater. Chem. A* **2017**, *5*, 11781.

[86] Y. Wang, W. Kang, D. Cao, M. Zhang, Z. Kang, Z. Xiao, R. Wang, D. Sun, *J. Mater. Chem. A* **2018**, *6*, 4776.

[87] L. Shi, D. Li, P. Yao, J. Yu, C. Li, B. Yang, C. Zhu, J. Xu, *Small* **2018**, *14*, 1802716.

[88] D. Xie, S. Cai, X. Sun, T. Hou, K. Shen, R. Ling, A. Fan, R. Zhang, S. Jiang, Y. Lin, *Inorg. Chem. Commun.* **2020**, *111*, 107635.

[89] S. Dong, C. Li, X. Ge, Z. Li, X. Miao, L. Yin, *ACS Nano* **2017**, *11*, 6474.

[90] B. Liu, D. Kong, Y. Wang, Y. V. Lim, S. Huang, H. Y. Yang, *FlatChem* **2018**, *10*, 14.

[91] S. Guan, T. Wang, X. Fu, L.-Z. Fan, Z. Peng, *Appl. Surf. Sci.* **2020**, *508*, 145241.

[92] Y. Huang, Z. Wang, Y. Jiang, S. Li, M. Wang, Y. Ye, F. Wu, M. Xie, L. Li, R. Chen, *Adv. Sci.* **2018**, *5*, 1800613.

[93] S. Yuvaraj, G. K. Veerasubramani, M.-S. Park, P. Thangavel, D.-W. Kim, *J. Alloys Compd.* **2020**, *821*, 153222.

[94] Y. Zhang, P. Wang, Y. Yin, X. Zhang, L. Fan, N. Zhang, K. Sun, *Chem. Eng. J.* **2019**, *356*, 1042.

[95] Y. Zhao, J. Wang, C. Ma, Y. Li, J. Shi, Z. Shao, *Chem. Eng. J.* **2019**, *378*, 122168.

[96] Y. Jiang, Y. Guo, W. Lu, Z. Feng, B. Xi, S. Kai, J. Zhang, J. Feng, S. Xiong, *ACS Appl. Mater. Interfaces* **2017**, *9*, 27697.

[97] X. Wang, X. Li, Q. Li, H. Li, J. Xu, H. Wang, G. Zhao, L. Lu, X. Lin, H. Li, S. Li, *Nano-Micro Lett.* **2018**, *10*, 46.

[98] Y.-Q. Wu, H.-X. Yang, Y. Yang, H. Pu, W.-J. Meng, R.-Z. Gao, D.-L. Zhao, *Small* **2019**, *15*, 1903873.

[99] C. Yang, X. Liang, X. Ou, Q. Zhang, H.-S. Zheng, F. Zheng, J.-H. Wang, K. Huang, M. Liu, *Adv. Funct. Mater.* **2019**, *29*, 1807971.

[100] C.-H. Lai, M.-Y. Lu, L.-J. Chen, *J. Mater. Chem.* **2012**, *22*, 19.

[101] S. C. Erwin, L. Zu, M. I. Haftel, A. L. Efros, T. A. Kennedy, D. J. Norris, *Nature* **2005**, *436*, 91.

[102] S. Huang, S. Fan, L. Xie, Q. Wu, D. Kong, Y. Wang, Y. V. Lim, M. Ding, Y. Shang, S. Chen, H. Y. Yang, *Adv. Energy Mater.* **2019**, *9*, 1901584.

[103] S. H. Woo, L. Yadgarov, R. Rosentsveig, Y. Park, D. Song, R. Tenne, S. Y. Hong, *Isr. J. Chem.* **2015**, *55*, 599.

[104] S. Bera, A. Roy, A. K. Guria, S. Mitra, N. Pradhan, *J. Phys. Chem. Lett.* **2019**, *10*, 1024.

[105] Y. Fang, D. Luan, Y. Chen, S. Gao, X. W. Lou, *Angew. Chem. Int. Ed.* **2020**, *59*, 2644.

Figures and Captions

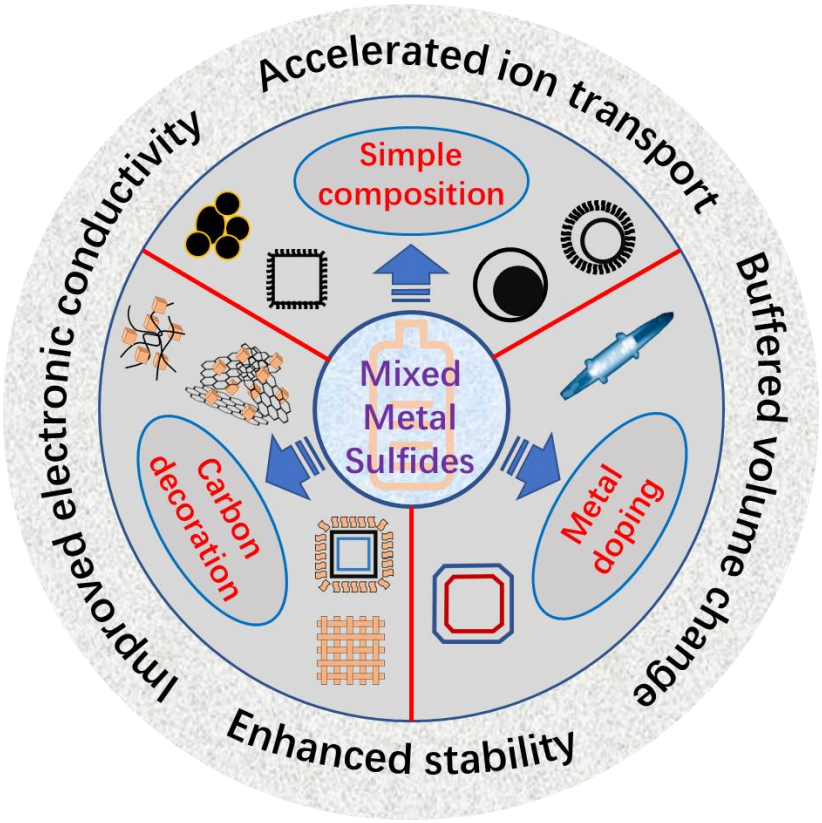

Figure 1. Overview of mixed metal sulfides for sodium-ion batteries.

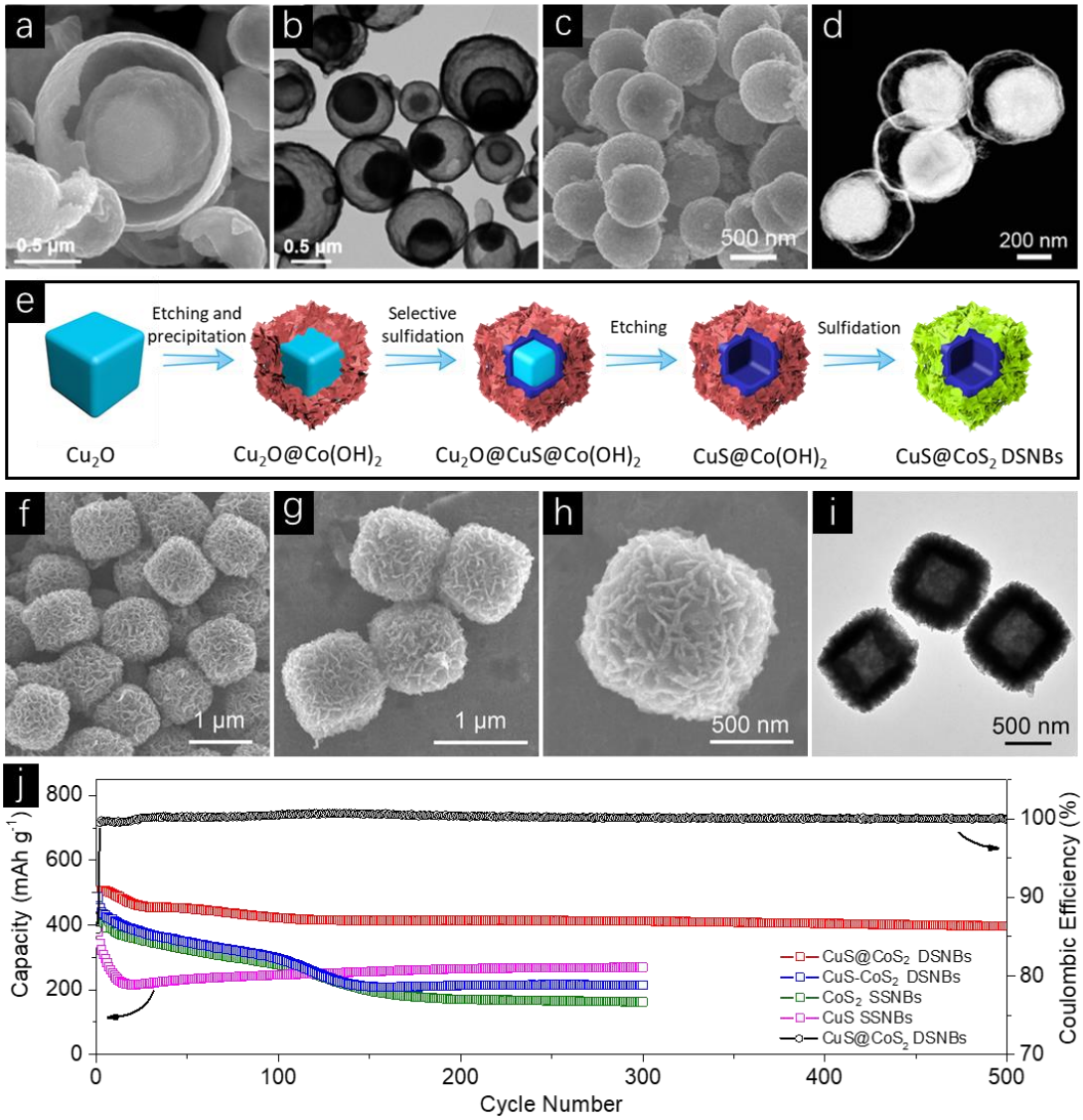

Figure 2. (a) FESEM and (b) TEM images of yolk-shelled SnS-MoS_2 microspheres. (c) FESEM and (d) HAADF-STEM images of yolk-shelled Co_9S_8/MoS_2 spheres. (e) Schematic illustration of the synthetic process of CuS@CoS_2 DSNBs. (f-h) FESEM and (i) TEM images of CuS@CoS_2 DSNBs. (j) Cycling performance of the CuS@CoS_2 DSNBs, CuS-CoS_2 DSNBs, CoS_2 SSNBs, and CuS SSNBs at a current density of 0.5 A g^{-1}. (a, b) Reproduced with permission.[44] Copyright 2015, American Chemical Society. (c, d) Reproduced with permission.[61] Copyright 2017, Wiley-VCH. (e-j) Reproduced with permission.[68] Copyright 2019, Wiley-VCH.

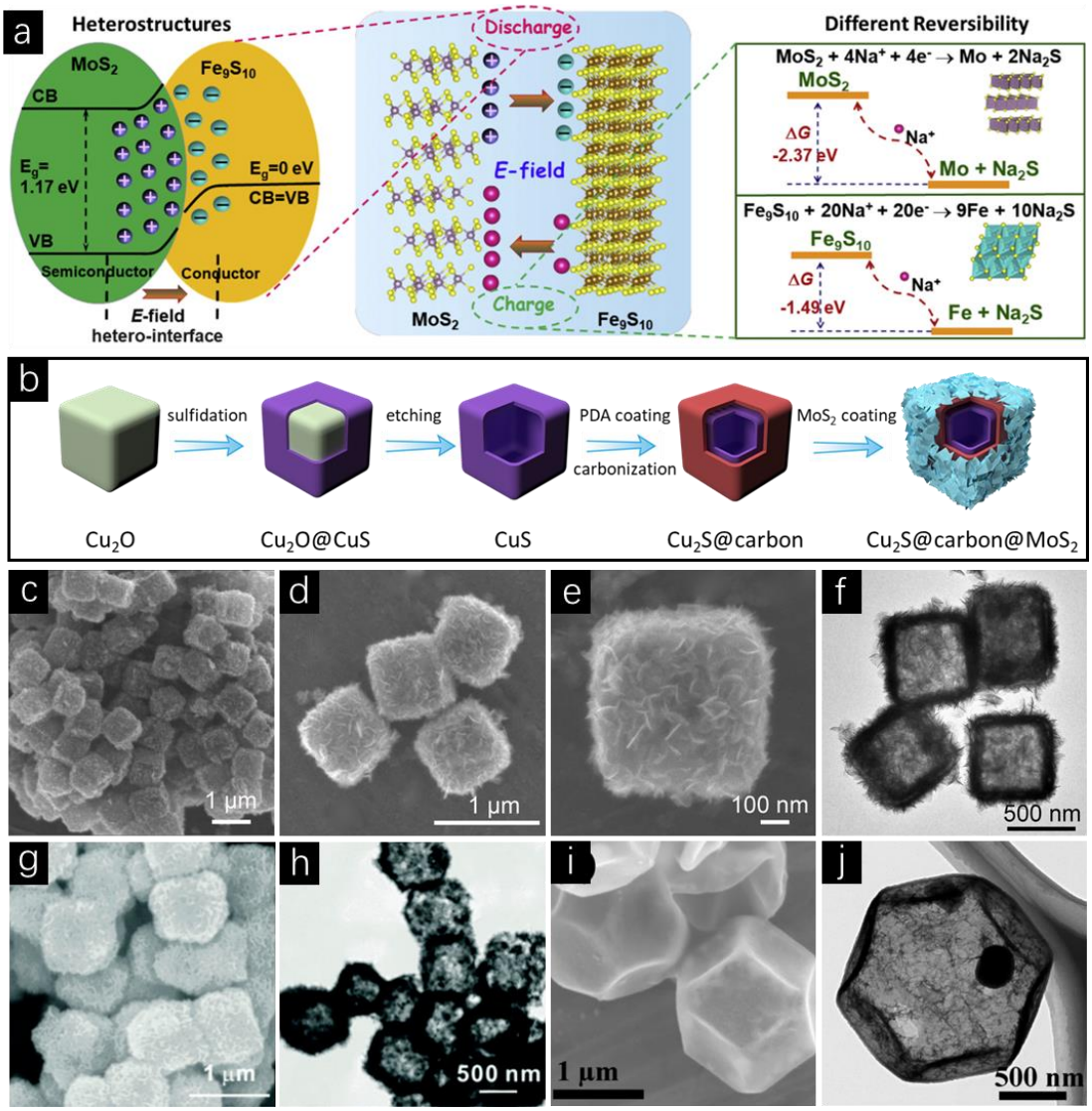

Figure 3. (a) Schematic illustration of the formation mechanism and direction of the internal electric field for Fe_9S_{10}@MoS_2@C during the discharge and charge processes. (b) Illustration of the synthetic process of the three-layered Cu_2S@carbon@MoS_2 nanoboxes. (c-e) FESEM and (f) TEM images of the three-layered Cu_2S@carbon@MoS_2 nanoboxes. (g) FESEM and (h) TEM images of MoS_2/Co_9S_8/C nanoboxes. (i) FESEM and (j) TEM images of ZnS-Sb_2S_3@C core-double shell polyhedron composite. (a) Reproduced with permission.[81] Copyright 2020, Elsevier. (b-f) Reproduced with permission.[82] Copyright 2020, Wiley-VCH. (g, h) Reproduced with permission.[84] Copyright 2017, Royal Society of Chemistry. (i, j) Reproduced with permission.[89] Copyright 2017, American Chemical Society.

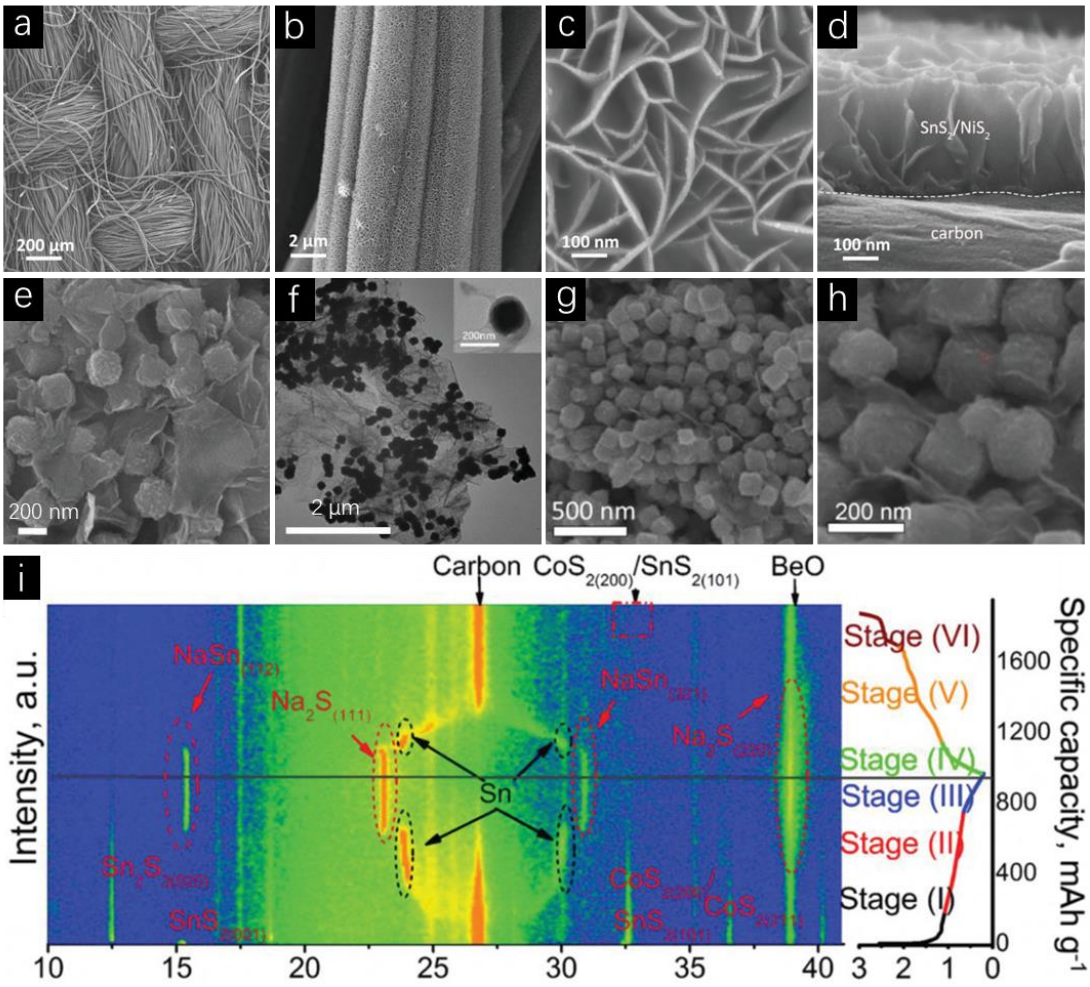

Figure 4. (a-d) FESEM images of the SnS_2/NiS_2@CC composite. (e) FESEM and (f) TEM images of the SnS_2/Co_3S_4-rGO composite. (g, h) FESEM images of the $(SnCo)S_2$/SG composite. (i) Count plot recorded at different sodiation/desodiation states against the electrochemical voltage during the initial cycle of the $(SnCo)S_2$/SG composite. (a-d) Reproduced with permission.[91] Copyright 2020, Elsevier. (e, f) Reproduced with permission.[98] Copyright 2019, Wiley-VCH. (g-i) Reproduced with permission.[99] Copyright 2019, Wiley-VCH.

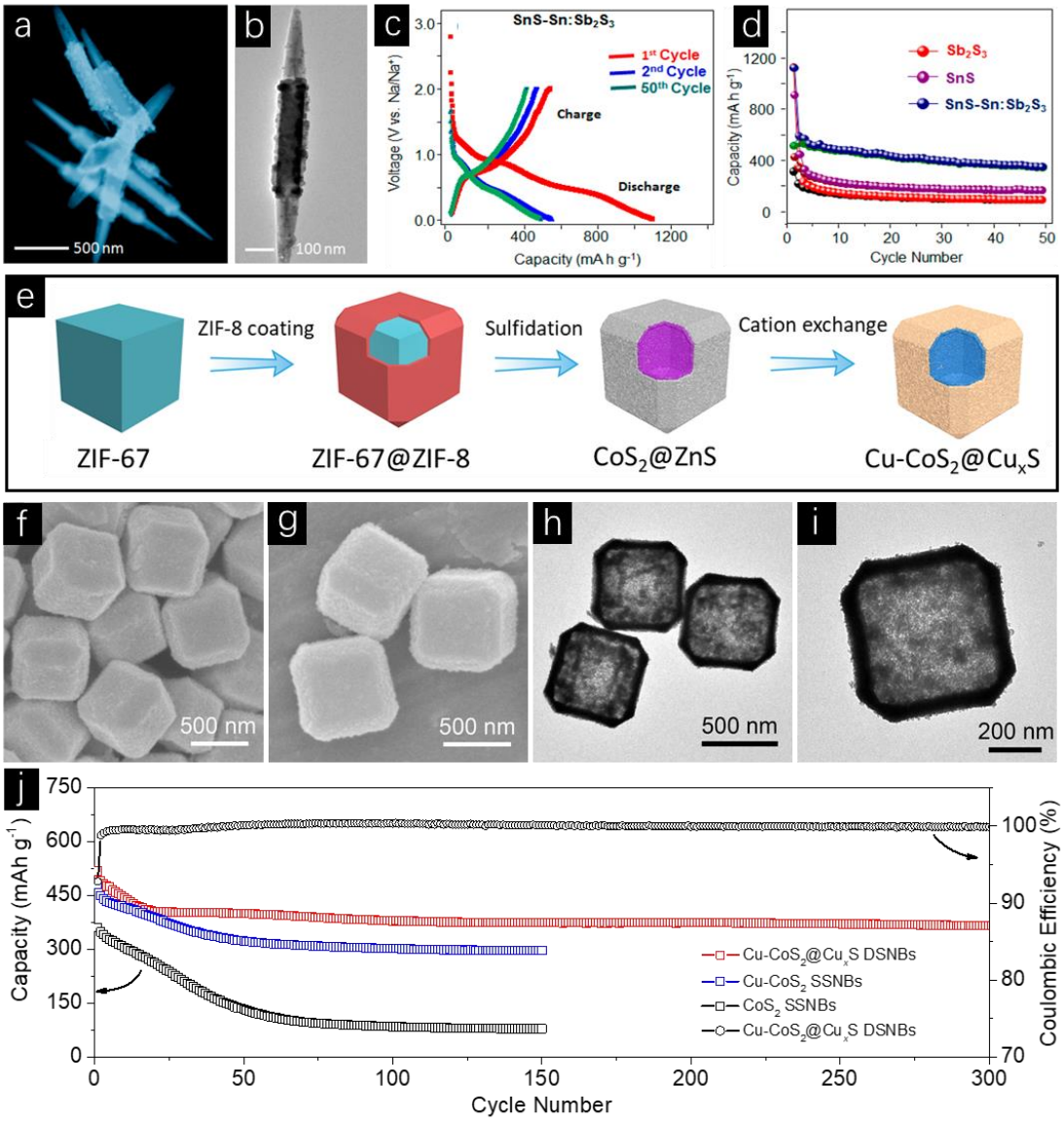

Figure 5. (a) HAADF-STEM and (b) TEM images of the SnS-Sn:Sb_2S_3 composite. (c) Galvanostatic charge-discharge profiles of the SnS-Sn:Sb_2S_3 electrode at a current density of 100 mA g^{-1}. (d) Comparison of cycling performances of the SnS-Sn:Sb_2S_3, Sb_2S_3, and SnS electrodes. (e) Synthetic process for the preparation of the Cu-CoS_2@Cu_xS DSNBs. (f, g) FESEM and (h, i) TEM images of Cu-CoS_2@Cu_xS DSNBs. (j) Cycling performance of the Cu-CoS_2@Cu_xS DSNBs, Cu-CoS_2 SSNBs, and CoS_2 SSNBs at a current density of 0.3 A g^{-1}. (a-d) Reproduced with permission.[104] Copyright 2019, American Chemical Society. (e-j) Reproduced with permission.[105] Copyright 2020, Wiley-VCH.

Table 1. Sodium storage performance of some MMSs based electrodes.

Materials	Cut-off voltage (V vs. Na/Na^+)	Reversible capacity (mAh g^{-1})/current density (A g^{-1})	Cycling stability (mAh g^{-1})/cycles/current density (A g^{-1})	Rate capability (mAh g^{-1})/current density (A g^{-1})	Ref.
Hierarchical Bi_2S_3/MoS_2 microspheres	0.1-3	558/0.1	323.4/1200/10	325.5/10	[42]
Yolk-shelled SnS-MoS_2 microspheres	0.001-2.5	453/0.2	396/100/0.5	238/7	[44]
$Fe_{1-x}S$/MnS nanocomposite	0.01-2.5	600/0.1	329/100/1	290/2	[58]
Yolk-shell Sn-Sb-S microflowers	0.01-3	921.7/0.1	607/50/0.1	98/2	[59]
Cobalt/zinc sulfides microflowers	0.01-3	444/0.1	294/600/0.5	231/10	[60]
Co_9S_8/MoS_2 yolk-shell spheres	0.01-3	500/0.3	300/1200/2	403/2	[61]
CuS@CoS_2 double-shelled nanoboxes	0.4-2.6	625/0.1	396/500/0.5	304/5	[68]
ZnS/Fe_9S_{10}@C nanoparticles	0.005-3	636/0.5	485/200/1	235/50	[43]
Co_9S_8/ZnS/C nanocrystals	0.01-3	529/0.1	219/500/10	259/10	[45]
CoS_2/Co_4S_3@N-doped carbon	0.01-3	650/0.3	239/3000/6	217/6	[55]
NiS/MoS_2/C hollow spheres	0.01-3	571/0.1	335/200/1	398/5	[70]
NiS_2@CoS_2@carbon nanocubes	0.01-3	660/0.1	600/250/1	560/5	[71]
Co-Sn-S@carbon nanoboxes	0.01-3	679/0.1	361/1000/1	478/10	[72]
Co_xS/Fe_xS@carbon nanoboxes	0.01-3	539.5/0.5	87/150/0.5	122/5	[73]
Carbon-coated NiS/MoS_2@ nanotubes	0.01-3	483/0.5	420/200/0.5	309/10	[74]
SnS_2/Mn_2SnS_4/carbon nanoboxes	0.1-3	841/0.1	523/500/5	489/10	[75]
SnS/ZnS@carbon nanocubes	0.01-2.5	639/0.2	485/250/0.2	400/2	[76]
$SnSbS_x$/carbon nanofiber	0.01-2.5	555/0.1	567/80/0.2	278.5/3.2	[77]
MoS_2-Ni_9S_8-C microspheres	0.001-3	462/0.1	366/80/0.5	428/3	[78]
ZnS/SnS_2@carbon nanoboxes	0.1-3	590/0.1	456/700/5	452/10	[79]
SnS@C/MoS_2@carbon nanospheres	0-3	628/1	220/2000/5	250/10	[80]

Fe_9S_{10}@MoS_2@carbon	0.005-3	521/0.2	355/1000/2	132/50	[81]
Cu_2S@carbon@MoS_2 nanoboxes	0.01-3	442/0.05	280/200/0.3	297/3	[82]
MnS-(ZnCo)S/N-C hollow polyhedron	0-3	532/1	353/400/2	170/10	[83]
MoS_2/Co_9S_8/C nanoboxes	0.01-3	634/0.5	546/100/0.5	222/10	[84]
Ni_3S_2/Co_9S_8/N-doped carbon hollow spheres	0.005-3	425/0.1	280/300/1	323/2	[85]
Yolk-shelled Co_9S_8/MoS_2-CN polyhedrons	0.01-3	604/0.5	438/150/1	421/2	[86]
CoS_2/C@SnS_2 nanoboxes	0.01-3	880/0.1	400/3500/10	620/5	[87]
FeS/ZnS/carbon nanoflower	0.01-3	585/0.1	475/50/0.1	208/2	[88]
ZnS-Sb_2S_3@C core-shelled polyhedron	0.01-1.8	1029/0.1	630/120/0.1	391/0.8	[89]
$NiCo_2S_4$@MoS_2 arrays	0.01-3	398/0.4	158/400/3.2	155/6.4	[90]
SnS_2/NiS_2 arrays	0-3	857/0.2	589/100/2	360/5	[91]
In_2S_3/Sb_2S_3@MCNTs	0.01-2.5	470/0.2	400/1000/0.4	355/3.2	[92]
FeS_2/MoS_2-rGO	0.01-3	468/0.1	459/150/0.1	347/3	[93]
SnS-ZnS@C nanoboxes	0.01-3	701/0.1	247/1000/2	267/20	[94]
FeS_2/FeS/MGN	0.01-3	552/0.1	513/100/0.1	251/20	[95]
MoS_2/SnS_2-GS	0.01-3	655/0.15	655/0.15/100	340/6	[96]
SnS_2@CoS_2-rGO	0.01-3	653/0.2	514/100/0.2	330/4	[97]
SnS_2/Co_3S_4-rGO	0.01-3	1309/0.1	846/100/0.5	393/10	[98]
(SnCo)S_2/SG	0.2-3	758/0.1	487/5000/5	469/10	[99]
SnS-Sn:Sb_2S_3	0.01-2	550/0.1	500/50/0.1	267/0.45	[104]
Cu-CoS_2@Cu_xS double-shelled nanoboxes	0.4-2.6	535/0.1	366/300/0.3	333/5	[105]

for Table of Content Entry

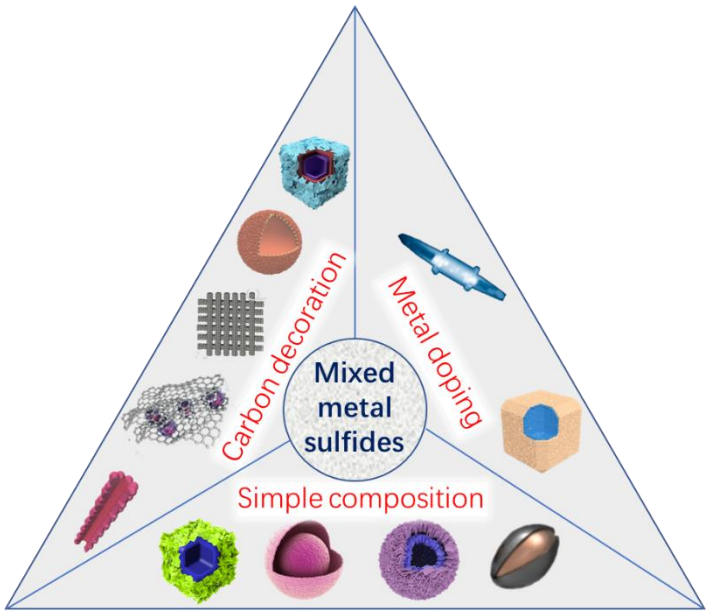

Mixed metal sulfides have been considered as promising negative electrode materials for sodium-ion batteries. This unique class of electrodes has some distinct advantages in boosting sodium storage properties. This Progress Report summarizes some recent advances in the rational design and synthesis of mixed metal sulfides as anode materials for sodium storage.